Two-dimensional electron gases induced by spontaneous and piezoelectric polarization charges in N- and Ga-face AlGaN/GaN heterostructures

O. Ambacher,[a] J. Smart, J. R. Shealy, N. G. Weimann, K. Chu, M. Murphy, W. J. Schaff, and L. F. Eastman
School of Electrical Engineering, Cornell University, Ithaca, New York 14853

R. Dimitrov, L. Wittmer, and M. Stutzmann
Walter Schottky Institute, TU-Munich, Am Coulombwall, 85748 Garching, Germany

W. Rieger and J. Hilsenbeck
Ferdinand Braun Institute, Rudower Chaussee 5, 12489 Berlin, Germany

(Received 24 September 1998; accepted for publication 13 December 1998)

Carrier concentration profiles of two-dimensional electron gases are investigated in wurtzite, Ga-face $Al_xGa_{1-x}N/GaN/Al_xGa_{1-x}N$ and N-face $GaN/Al_xGa_{1-x}N/GaN$ heterostructures used for the fabrication of field effect transistors. Analysis of the measured electron distributions in heterostructures with AlGaN barrier layers of different Al concentrations ($0.15<x<0.5$) and thickness between 20 and 65 nm demonstrate the important role of spontaneous and piezoelectric polarization on the carrier confinement at GaN/AlGaN and AlGaN/GaN interfaces. Characterization of the electrical properties of nominally undoped transistor structures reveals the presence of high sheet carrier concentrations, increasing from 6×10^{12} to $2\times10^{13}\,cm^{-2}$ in the GaN channel with increasing Al-concentration from $x=0.15$ to 0.31. The observed high sheet carrier concentrations and strong confinement at specific interfaces of the N- and Ga-face pseudomorphic grown heterostructures can be explained as a consequence of interface charges induced by piezoelectric and spontaneous polarization effects. © *1999 American Institute of Physics.*
[S0021-8979(99)04106-7]

I. INTRODUCTION

AlGaN/GaN heterostructure field-effect transistors (HFETs) have been a subject of intense recent investigation and have emerged as attractive candidates for high voltage, high-power operation at microwave frequencies.[1–6] Although the electron effective mass in GaN is 0.22, which is about three times higher than the effective electron mass in GaAs and as a result the low-field mobility of bulk GaN is much less than that of GaAs, GaN has a larger peak electron velocity, larger saturation velocity, higher thermal stability, and a larger band gap, very suitable for the use as channel-material in microwave power devices. Further contributing to the outstanding performance of AlGaN/GaN based HFETs is the ability to achieve two-dimensional electron gases (2DEG) with sheet carrier concentrations of $10^{13}\,cm^{-2}$ or higher close to the interface without intentionally doping, well in excess of those achievable in other III–V material systems. It has been shown previously that piezoelectric effects can exert a substantial influence on charge density and electric field distributions in strained zincblende semiconductors grown in the (111) orientation,[7] and more recently in strained or pseudomorphic group-III-nitride heterostructures with the wurtzite crystal structure grown in the (0001) orientation.[8] Especially in wurtzite AlGaN/GaN based transistor structures, the piezoelectric polarization of the strained top layer is more than five times larger as compared to AlGaAs/GaAs structures, leading to a significant increase of the sheet carrier concentration at the interface.[9–13] Bernardini *et al.*[14] pointed out that, in addition to the high piezoelectric polarization, the spontaneous polarization (polarization at zero strain) is very large in wurtzite group-III-nitrides, particularly AlN possesses a spontaneous polarization only about 3–5 times smaller than that of typical ferroelectric perovskites.[15] The spontaneous and piezoelectric polarization in wurtzite GaN and AlN are found to be ten times larger than in conventional III–V and II–VI semiconductor compounds and are comparable to those of ZnO. The spontaneous polarization can cause electric fields of up to 3 MV/cm in group-III-nitride crystals, and strain in pseudomorphically grown AlGaN/GaN or lnGaN/GaN heterostructures can cause an additional piezoelectric field of about 2 MV/cm. These very high polarizations and resulting electric fields produce high interface charge densities at group-III-nitride interfaces and spatial separation of the hole and electron wave functions in GaN-based quantum well structures.[16]

In this article, we will focus on the electrical and structural characterization of AlGaN/GaN/AlGaN and GaN/AlGaN/GaN heterostructures grown by metalorganic chemical vapor deposition (MOCVD) and plasma induced molecular beam epitaxy (PIMBE) to understand the formation of 2DEGs induced by spontaneous and piezoelectric polarization. Furthermore, we will elaborate on the important role of the polarity on the confinement and localization of 2DEGs inside group-III-nitride heterostructures suitable for the fabrication of high power field effect transistors. Finally,

[a]Electronic mail: ambacher@iiiv.tn.cornell.edu

 © 1999 American Institute of Physics

Downloaded 28 Mar 2002 to 128.111.29.147. Redistribution subject to AIP license or copyright, see http://ojps.aip.org/japo/japcr.jsp

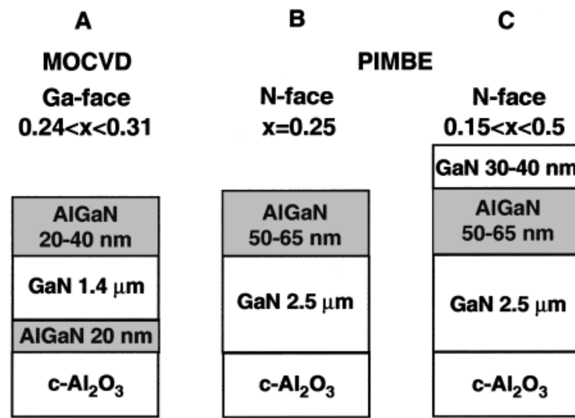

FIG. 1. Schematic drawing of the AlGaN/GaN based heterostructures grown by MOCVD and PIMBE on c-Al_2O_3 substrates.

we will calculate the polarization induced sheet charge and sheet carrier concentration at AlGaN/GaN and GaN/AlGaN interfaces and compare our results with published experimental and theoretical data.

II. GROWTH AND STRUCTURAL QUALITY OF AlGaN/GaN HETEROSTRUCTURES

The investigated epitaxial GaN layers, AlGaN/GaN, AlGaN/GaN/AlGaN, and GaN/AlGaN/GaN heterostructures are grown by MOCVD and PIMBE on c-plane sapphire substrates. The MOCVD grown GaN-based layers and heterostructures (heterostructure A, Fig. 1) are deposited at a pressure of 100 mbar, using triethylgallium (TEG), trimethylaluminium (TMA), and ammonia as precursors. A high-temperature AlGaN nucleation layer with a thickness of about 20 nm is deposited before the growth of GaN. Epitaxial GaN films deposited with rates of up to 1.5 μm/h show surfaces with bilayer steps (surface roughness rms$\approx$0.2 nm) and a few nanopipes. The measured free carrier concentration and Hall-mobility at room temperature are $2\times 10^{16}\,\mathrm{cm}^{-3}$ and 600 cm^2/V s for a sample thicknesses of 1.4 μm. By decreasing the flow ratio of TEG to TMA, the Al-content increases from 0.2 to 0.31, and the thickness of the barrier increases from 20 to 40 nm.[17]

Additionally, GaN films, AlGaN/GaN, and GaN/AlGaN/GaN heterostructures (Fig. 1, structures B and C) are deposited by PIMBE using a Tectra molecular-beam epitaxy MBE® chamber with a background pressure of 5×10^{-11} mbar, conventional effusion cells, and an Oxford Applied Research CARS 25 r.f. plasma source for the generation of nitrogen radicals. The nitrogen flux through the plasma source is fixed at 2 sccm causing a nitrogen partial pressure in the MBE chamber of 4×10^{-5} mbar during growth. The samples are rotated at a rate of 20 rpm to obtain homogeneous films over 2 in. (0001) Al_2O_3 substrates. The optimized growth temperature T_s for GaN and $Al_xGa_{1-x}N$ $(0<x<0.5)$ was determined to be $T_s=132\,°\mathrm{C}\,x+780\,°\mathrm{C}$ at a deposition rate of 0.6 μm/h.[6]

Besides the substrate temperature, the optimization of the Ga-flux under metal-rich growth conditions was found to be most important for the growth of GaN with high electron mobility. By increasing the Ga-flux from $8\times 10^{14}\,\mathrm{cm}^{-2}\,\mathrm{s}^{-1}$ to $1.5\times 10^{15}\,\mathrm{cm}^{-2}\,\mathrm{s}^{-1}$ and keeping all other deposition parameters constant, the electron mobility at room temperature for 1 μm-thick-films was increased from 50 to 250 cm^2/V s, whereas the concentration of free carriers dropped from 5×10^{17} to $8\times 10^{16}\,\mathrm{cm}^{-3}$. A further improvement of the mobility to 550 cm^2/V s at room temperature and 750 cm^2/V s at 77 K was realized by increasing the thickness of the GaN film to 2.5 μm. The carrier density for nominally undoped samples was about $4.5\times 10^{16}\,\mathrm{cm}^{-3}$ at room temperature and $1\times 10^{16}\,\mathrm{cm}^{-3}$ at 77 K. The improvement of electrical properties by increasing the Ga-flux coincides with a reduction of structural defects, as determined by high resolution x-ray diffraction measurements (HRXRD) and atomic force microscopy. Our best GaN films grown by PIMBE without nucleation layers exhibited a full width at half maximum of 250 arc s (rocking curve) and a surface roughness rms$<$2 nm for 2.5 μm-thick-films.

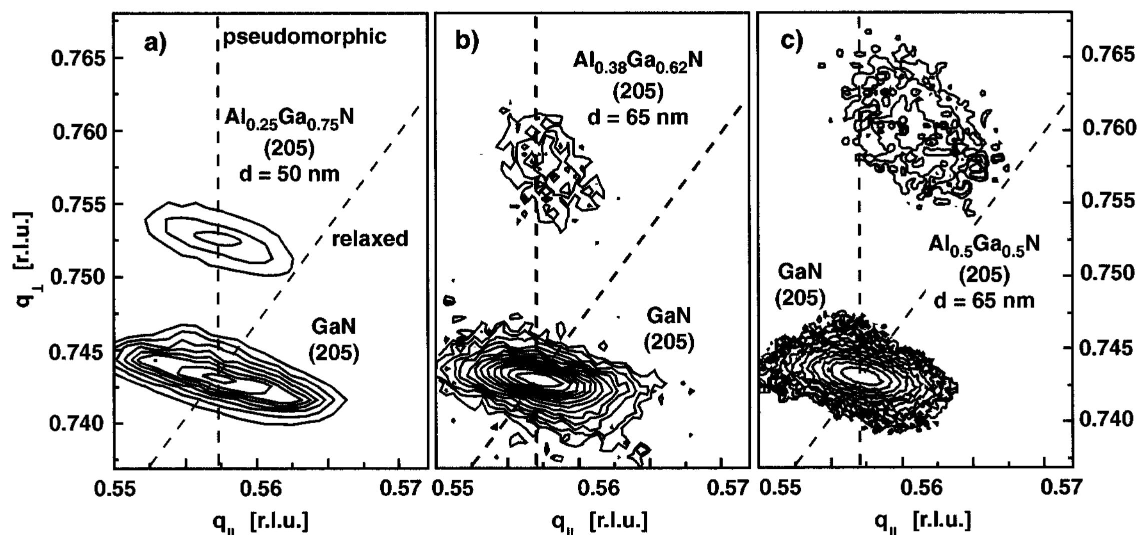

FIG. 2. Reciprocal space maps of the 20.5 reflections of AlGaN/GaN heterostructures measured by HRXRD. The position of the x-ray diffraction reflections for relaxed and pseudomorphic grown AlGaN with different alloy compositions are shown as dashed lines.

Downloaded 28 Mar 2002 to 128.111.29.147. Redistribution subject to AIP license or copyright, see http://ojps.aip.org/japo/japcr.jsp

TABLE I. Structural parameters, Bohr radius, and binding energy for AlN, GaN, and InN.

Wurtzite, 300 K	AlN	GaN	InN
a_0 [Å][b]	3.112	3.189	3.54
c_0 [Å][b]	4.982	5.185	5.705
c_0/a_0 (exp)[b]	1.6010	1.6259	1.6116
c_0/a_0 (cal)[a]	1.6190	1.6336	1.6270
u_0[a]	0.380	0.376	0.377
a_{Bohr} [Å][a]	5.814	6.04	6.66
$E_B(M-N)$ [eV][b]	2.88	2.20	1.98

[a]Ref. 14.
[b]Ref. 18.

AlGaN alloys were grown using the optimized flux of Ga-metal atoms for the total flux of group III atoms. For Si-doped AlGaN with an Al-content of 25%, we obtained an electron mobility of 70 $\mathrm{cm^2/V\,s}$ at a doping level of $1.5\times10^{19}\,\mathrm{cm^{-3}}$. The good electrical properties of GaN and Si-doped AlGaN motivated the PIMBE growth of nominal undoped AlGaN/GaN and GaN/AlGaN/GaN heterostructures shown in Fig. 1. Structure B is similar to the typical MOCVD grown AlGaN/GaN HFET heterostructure A, but lacks a nucleation layer. The heterostructure contains a 2.5 μm thick GaN buffer layer and a 50 or 65 nm $Al_xGa_{1-x}N$ undoped cap layer with Al contents between 0.15 and 0.5. The AlGaN film is thick in comparison to typical transistor structures ($d_{\mathrm{AlGaN}}=15-30\,\mathrm{nm}$) to enable the determination of strain and Al-content by HRXRD. The first two layers of structures B and C are similar. In addition, heterostructure C is capped by a 30 nm thick undoped GaN.

In order to determine the precise composition x of the strained AlGaN layers in heterostructures B and C, reciprocal space maps of the symmetric (20.0) and asymmetric (20.5) reflexes (Fig. 2) of the AlGaN/GaN and GaN/AlGaN/GaN heterostructures are measured by HRXRD, and the alloy composition is calculated using the lattice constants and elastic stiffness shown in Table I and Table II for each binary compound.[24,25] Although the thickness of the AlGaN layers ($d_{\mathrm{AlGaN}}=65\,\mathrm{nm}$) grown on GaN is above the critical layer thickness estimated from the Matthews–Blakeslee model[26] or Fischer model[27] for $x>0.15$, pseudomorphic growth is observed up to $x=0.34$, which is in agreement with the data published by H. Amano *et al.*[28] Even up to $x=0.38$ pseudomorphic growth is observed, but the lattice constant a(GaN) is slightly decreased by 0.0005 nm (Fig. 3). The structural quality decreases and partial relaxation of the AlGaN layer occurs for $x=0.5$ (Fig. 2).

TABLE II. Measured and calculated elastic constants of wurtzite and cubic AlN, GaN, and InN.

GPa wurtzite	AlN exp.[a]	AlN cal.[b]	GaN exp.[c]	GaN cal.[b]	InN exp.[d]	InN cal.[b]
c_{11}	345	396	374	367	190	223
c_{12}	125	137	106	135	104	115
c_{13}	120	108	70	103	121	92
c_{33}	395	373	379	405	182	224
c_{44}	118	116	101	95	10	48
B	201	207	180	202	139	141
zincblende	cal.[e]	cal.[b]	cal.[e]	cal.[b]	cal.[e]	cal.[b]
c_{11}	304	304	296	293	184	187
c_{12}	152	160	154	159	116	125
c_{44}	199	193	206	155	177	86

[a]Ref. 19.
[b]Ref. 20.
[c]Ref. 21.
[d]Ref. 22.
[e]Ref. 23.

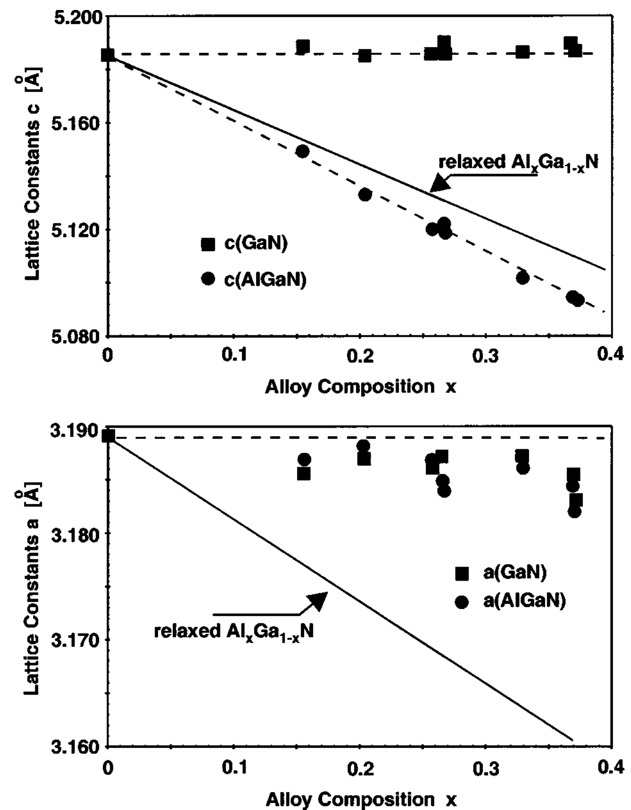

FIG. 3. Measured lattice constants a and c of GaN and AlGaN layers part of a pseudomorphic grown GaN/AlGaN/GaN heterostructures. The dashed and the solid line indicate the lattice constants vs Al-content of the AlGaN layer for a pseudomorphic and relaxed grown barrier.

The piezoelectric polarization, the polarization induced charge density, and the sheet carrier density calculated later on will be determined for pseudomorphic grown heterostructures. Because of the measured lattice constants and strain of the AlGaN/GaN and GaN/AlGaN/GaN structures, we have to expect good agreement between the theoretical and experimental results as long as $x<0.38$ and $d_{\mathrm{AlGaN}}\leq65\,\mathrm{nm}$.

Before the influence of piezoelectric and spontaneous polarization on the carrier confinement at the AlGaN/GaN interfaces can be calculated, we will discuss the directions of the polarizations which are influenced by the polarity of the crystals.

III. POLARITY

Noncentrosymmetric compound crystals exhibit two different sequences of the atomic layering in the two opposing directions parallel to certain crystallographic axes, and consequently crystallographic polarity along these axes can be

Downloaded 28 Mar 2002 to 128.111.29.147. Redistribution subject to AIP license or copyright, see http://ojps.aip.org/japo/japcr.jsp

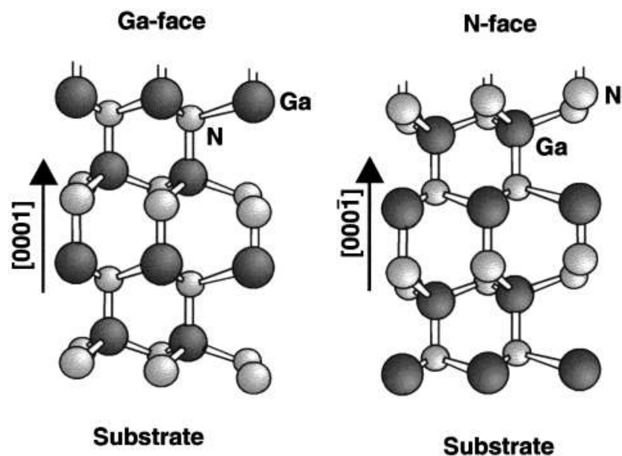

FIG. 4. Schematic drawing of the crystal structure of wurtzite Ga-face and N-face GaN.

observed. For binary A–B compounds with wurtzite structure, the sequence of the atomic layers of the constituents A and B is reversed along the [0001] and [000$\bar{1}$] directions. The corresponding (0001) and (000$\bar{1}$) faces are the A-face and B-face, respectively. In the case of heteroepitaxial growth of thin films of a noncentrosymmetric compound, the polarity of the material cannot be predicted in a straightforward way, and must be determined by experiments. This is the case for GaN epitaxial layers and GaN-based heterostructures with the most common growth direction normal to the {0001} basal plane, where the atoms are arranged in bilayers. These bilayers consist of two closely spaced hexagonal layers, one formed by cations and the other formed by anions, leading to polar faces. Thus, in the case of GaN, a basal surface should be either Ga- or N-faced. By Ga-faced we mean Ga on the top position of the {0001} bilayer, corresponding to the [0001] polarity (Fig. 4) (by convention, the **z** or [0001] direction is given by a vector pointing from a Ga atom to a nearest-neighbor N atom). It is, however, important to note that the (0001) and (000$\bar{1}$) surfaces of GaN are nonequivalent and differ in their chemical and physical properties.[29]

Both types of polarity were reported to be found by ion channeling and convergent beam electron diffraction in GaN (0001) layers grown by MOCVD on *c*-plane sapphire if the layers exhibited rough morphology, while for smooth films Ga-face was exclusively concluded from the experimental results.[30] This result was supported by a photoelectron diffraction study of MOCVD grown films.[31] Smith *et al.*[32,33] reported on investigations of surface reconstructions of GaN grown by PIMBE on *c*-plane sapphire and PIMBE homoepitaxy on a MOCVD grown GaN sapphire substrate. They observed two structurally nonequivalent faces with completely different surface reconstructions attributed to the N-face for MBE on sapphire and to the Ga-face for MBE on a MOCVD template.

Weyher *et al.*[34] studied the etching of GaN crystals and MOCVD GaN films in aqueous solutions of KOH and NaOH. They found that the rough surface of MOCVD films with hexagonal crystallites (N-face)[31] etched much more easily than the smooth Ga-face, related to the finding of Sasaki *et al.*[35] that rough films (N-face) oxidize more easily.

We used the x-ray standing wave method (XSW) and chemical etching to determine the polarity of the MOCVD and PIMBE grown films. The advantage of the XSW technique lies in the combination of the structural sensitivity of x-ray diffraction with the chemical elemental sensitivity inherent to x-ray spectroscopy.[36] The method is based on generating an XSW field by x-ray Bragg diffraction and monitoring the x-ray fluorescence yield excited by this field as a function of glancing angle as the GaN layer is turned through the narrow region of Bragg reflection. Determining the polarity of noncentrosymmetric crystals with the XSW technique is straight forward and has been demonstrated for GaP[37,38] and GaAs.[39,40] In the case of a wurtzite GaN film with a thickness of 1 μm grown by PIMBE (similar to the first layer of structures B and C) without nucleation layer, the XSW technique was successfully applied. The standing wave was generated by x-ray diffraction inside the GaN film and the Ga $K\alpha$ fluorescence yield was recorded as a function of the incidente angle within the width of the (0002) reflection peak. In these studies, N-face was found predominantly. The uncertainty of the measurement allows for 10% fraction of Ga-face material, at most. However, the sharpness of the Bragg-peak indicates high structural film quality (for further details see Ref. 41).

Chemical etching of the GaN film grown by PIMBE for 10 min at 80 °C in a 1:10 KOH:H_2O solution increased the rms surface roughness from 2 to about 7 nm, whereas the MOCVD grown GaN films with a surface roughness of rms$\approx$0.2 nm were stable over more than 30 min under the same conditions.

As observed by XSW and chemical etching, we conclude that our PIMBE grown GaN films are of N-face, while our MOCVD grown films are of Ga-face material, in agreement with the observations made by other groups mentioned above. Because there are no theoretical and experimental results, that the face of an AlGaN/GaN heterostructure can be different from the GaN bottom layer, it can be concluded that structure A (Fig. 1) must possess the Ga(Al)-face, and heterostructures B and C must be of N-face polarity material.

In the following, the influence of the different polarities on the electrical properties of AlGaN/GaN based structures will be discussed.

IV. CARRIER CONFINEMENT AND TWO-DIMENSIONAL ELECTRON GASES

Modulation doping, e.g., doping of the AlGaAs barrier layer close to an AlGaAs/GaAs heterointerface, induces carriers in the undoped channel region. In the case of *n*-type doping of the barrier, the region in the barrier close to the interface will be depleted, and the corresponding electrons will accumulate in a triangular shaped potential in the GaAs layer close to the interface. The electrons accumulated in the potential will form a two-dimensional electron gas. These electrons have an increased mobility in comparison to electrons in the bulk of the active layer, since the carriers are spatially separated from dopants in the barrier layer.[42,43] This fact is frequently used for device applications in HFETs.

Downloaded 28 Mar 2002 to 128.111.29.147. Redistribution subject to AIP license or copyright, see http://ojps.aip.org/japo/japcr.jsp

Even at interfaces of intentionally undoped AlGaN/GaN heterostructures with high structural quality the formation of a 2DEG can be expected because of the free carrier background concentration in the active GaN and the AlGaN barrier layers or carrier injection from metal contacts. Hall measurements using van der Pauw configuration and Ti/Al metalization for ohmic contacts are used to determine the electron mobility and the sheet carrier concentration of the 2DEG. For structure A (MOCVD, $d_{\mathrm{AlGaN}}=20\,\mathrm{nm}$), the electron sheet concentration and the mobility at room temperature increased from 6.2×10^{12} to $1.1\times10^{13}\,\mathrm{cm}^{-2}$, and 540 to 800 $\mathrm{cm}^2/\mathrm{V\,s}$, respectively, by increasing the Al content x of the AlGaN barrier from $x=0.24$ to 0.31. For structure B (PIMBE) Hall measurements yielded a sheet carrier concentration and mobility of $2.7\times10^{12}\,\mathrm{cm}^{-2}$ and 350 $\mathrm{cm}^2/\mathrm{V\,s}$ at 300 K, and $4.4\times10^{11}\,\mathrm{cm}^{-2}$ and 345 $\mathrm{cm}^2/\mathrm{V\,s}$ at 77 K, respectively. Carrier confinement or a two-dimensional electron gas was not observed in structure B. In structure C grown by PIMBE (inverted structure), the carrier concentration for a barrier with $x=0.2$ decreased only slightly from 7.4×10^{12} to $6.5\times10^{12}\,\mathrm{cm}^{-2}$, but the mobility increased significantly from 1000 to 2000 $\mathrm{cm}^2/\mathrm{V\,s}$ by lowering the measurement temperature from 300 to 77 K. The constant electron sheet concentration and the drastic improvement in the electron mobility indicate spatial confinement of carriers, and the formation of a 2DEG in this structure. By increasing the Al-mole fraction to 0.26, the sheet carrier concentration of the 2DEG increased to 1.2×10^{13} and $1.1\times10^{13}\,\mathrm{cm}^{-2}$ (mobility 830 and 1510 $\mathrm{cm}^2/\mathrm{V\,s}$) at room temperature and 77 K, respectively.

To determine at which interface of structure C the electrons are confined, the upper 30 nm of the Hall sample was removed by reactive ion etching using BCl_3. After the etching, a low electron sheet density of $4\times10^{12}\,\mathrm{cm}^{-2}$ and mobility of 200 $\mathrm{cm}^2/\mathrm{V\,s}$ was measured, indicating that the 2DEG is confined at the upper GaN/AlGaN interface for the PIMBE grown material.

To find additional information about the sheet carrier concentration and at which interface the 2DEGs are confined, we applied the capacitance–voltage ($C-V$) profiling technique[44] using a multifrequency inductance, capacitance, resistivity (LCR) meter operated at room temperature between 10 and 20 kHz and a mercury probe with a contact area of 750 $\mu\mathrm{m}^2$. The $C-V$ profiling technique allows one to measure the carrier concentration

$$N_{C-V}=\frac{C^3}{e\epsilon_0\epsilon}\frac{dV}{dC}, \tag{1}$$

as a function of depth

$$z_{C-V}=\frac{\epsilon_0\epsilon}{C}, \tag{2}$$

where V is the voltage applied to the Schottky contact (mercury), C is the measured differential capacitance per unit area, and ϵ is the dielectric constant of the material ($\epsilon_0=8.85\times10^{-14}C/V\,\mathrm{cm}$; $e=1.602\times10^{-19}C$). In the simplest case, that is for a noncompensated, homogeneously doped semiconductor, the $C-V$-concentration N_{C-V} equals the free carrier concentration. In semiconductors and heterostructures with large variations of the doping concentration, and espe-

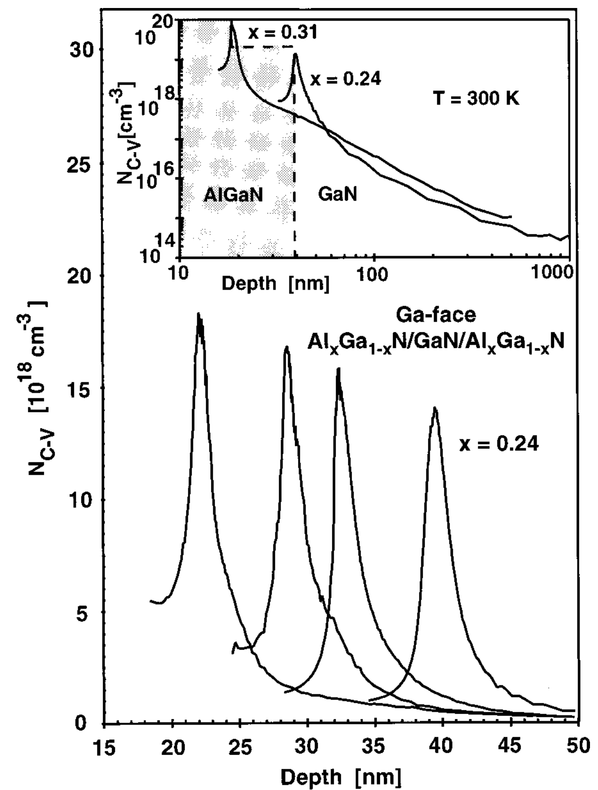

FIG. 5. $C-V$-concentration profile N_{C-V} vs penetration depth of $Al_{0.24}Ga_{0.76}N$/GaN/AlGaN heterostructures grown by MOCVD with thicknesses of the barrier between 20 and 40 nm measured by $C-V$-profiling technique. The insert shows N_{C-V} vs depth on a logarithmic scale for heterostructures with alloy compositions of $x=0.24$ and 0.31. The 2DEG is located at the upper AlGaN/GaN interface.

cially in structures with quantum confinement, the $C-V$-concentration does not have a direct physical meaning. However, N_{C-V} corresponds approximately to the free carrier concentration $N_{C-V}(z)\cong n(z)$.[45] Nevertheless, Kroemer *et al.*[46] showed that charge conservation is fulfilled for $C-V$-profiles, that is,

$$n_S=\int_{-\infty}^{\infty}N_{C-V}(z_{C-V})dz_{C-V}=\int_{-\infty}^{\infty}n(z)dz.$$

This property of the $C-V$-technique is very useful and enables the determination of the sheet carrier concentration n_S and of the location of the 2DEG in the AlGaN/GaN heterostructures. In Fig. 5, the measured $N_{C-V}(z_{C-V})$ profiles are shown for structure A with $Al_{0.24}Ga_{0.76}N$ barrier thicknesses between 20 and 40 nm. A slight increase of n_S from 6×10^{12} to $9\times10^{12}\,\mathrm{cm}^{-2}$ with increasing thickness of the barrier is detected. We found an increase of the sheet carrier concentration to $1.5\times10^{13}\,\mathrm{cm}^{-2}$ by increasing the Al-content to $x=0.31$ ($d_{\mathrm{AlGaN}}=20\,\mathrm{nm}$). This is in good agreement with the results of the Hall measurements. More importantly, the localization of the 2DEG inside the MOCVD grown Ga-face heterostructure is determined to be at the upper AlGaN/GaN interface (insert of Fig. 5), similar to the observations by Yu *et al.* using $C-V$-measurements.[47] $N_{C-V}(z_{C-V})$ profiles for inverted structure C with d_{AlGaN} between 30 and 40 nm and Al-contents of 0.17, 0.2, and 0.26 are shown in Fig. 6. Again we observe very high sheet carrier concentrations increasing

Downloaded 28 Mar 2002 to 128.111.29.147. Redistribution subject to AIP license or copyright, see http://ojps.aip.org/japo/japcr.jsp

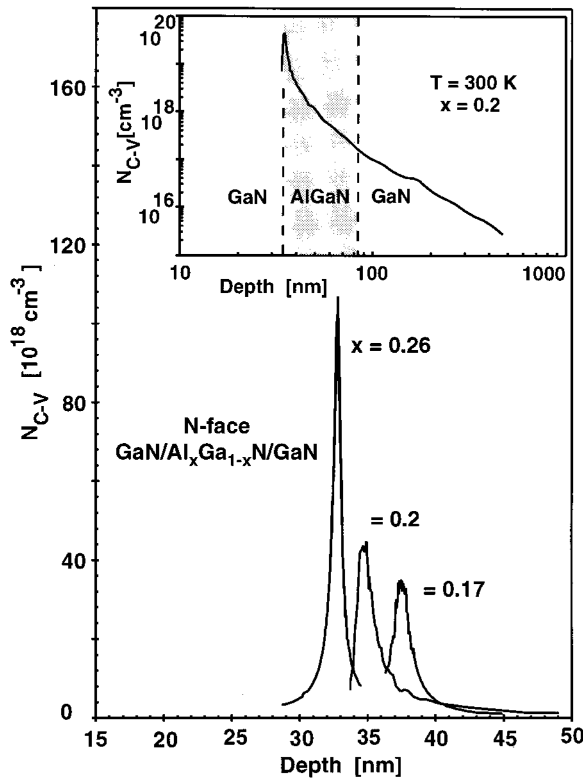

FIG. 6. $C-V$-concentration profile N_{C-V} vs penetration depth of GaN/Al$_x$Ga$_{1-x}$N/GaN heterostructures grown by PIMBE with Al-contents of the barrier between $x=0.17$ and 0.26 measured by $C-V$-profiling technique. The insert shows N_{C-V} vs depth on a logarithmic scale for a heterostructure with an alloy composition of $x=0.2$. The 2DEG is located at the upper GaN/AlGaN interface.

from 7.8×10^{12} to 1.3×10^{13} if the Al-content is increased. But opposite to the heterostructures grown by MOCVD, the 2DEG is located at the upper GaN/AlGaN interface of the N-face GaN/AlGaN/GaN heterostructure. In structures B and C no carrier accumulation could be detected at the AlGaN/GaN interface, although the structural quality of the layer and interface was found to be very similar.

As a consequence of the experimental observations the following questions arise:

(i) What are the reasons for the very high sheet carrier densities at one of the interfaces of the undoped heterostructures?

(ii) Why are the carriers forming a 2DEG located at different interfaces inside the Ga-face (MOCVD) and N-face (PIMBE) heterostructures?

To answer these questions, we have to understand the role of effects induced by spontaneous and piezoelectric polarization in heterostructures with different polarities in more detail.

V. SPONTANEOUS AND PIEZOELECTRIC POLARIZATION

In the absence of external electric fields, the total macroscopic polarization **P** of a GaN or AlGaN layer is the sum of the spontaneous polarization $\mathbf{P}_{\mathrm{SP}}$ in the equilibrium lattice,

TABLE III. Spontaneous polarization, piezoelectric and dielectric constants of AlN, GaN, and InN.

wurtzite	AlN	GaN	InN
P_{SP} [C/m^2]	−0.081	−0.029	−0.032
	1.46[a]	0.73[a]	0.97[a]
e_{33}	1.55[b]	1[c]	
[C/m^2]		0.65[d]	
		0.44[e]	
e_{31}	−0.60[a]	−0.49[a]	−0.57[a]
[C/m^2]	−0.58[b]	−0.36[c]	
		0.33[d]	
		−0.22[e]	
e_{15}	−0.48[b]	−0.3[c]	
[C/m^2]		−0.33[d]	
		−0.22[e]	
ϵ_{11}	9.0[b]	9.5[f]	
ϵ_{33}	10.7[b]	10.4[f]	

[a]Ref. 14.
[b]Ref. 47.
[c]Ref. 48.
[d]Ref. 49.
[e]Ref. 50.
[f]Ref. 51.

and the strain-induced or piezoelectric polarization $\mathbf{P}_{\mathrm{PE}}$. Because of the sensitive dependence of the spontaneous polarization on the structural parameters, there are some quantitative differences in the polarization for GaN and AlN. The increasing nonideality of the crystal structure going from GaN to AlN [u_0 being the anion-cation bond length along the (0001) axis in units of c increases, c/a decreases (Table I)] corresponds to an increase in spontaneous polarization. Here we consider polarizations along the [0001] axis, since this is the direction along which epitaxial films and AlGaN/GaN heterostructures are grown. The spontaneous polarization along the c-axis of the wurtzite crystal is $\mathbf{P}_{\mathrm{SP}}=P_{\mathrm{SP}}\mathbf{z}$. The piezoelectric polarization can be calculated with the piezoelectric coefficients e_{33} and e_{13} (Table III) as

$$P_{\mathrm{PE}}=e_{33}\epsilon_z+e_{31}(\epsilon_x+\epsilon_y), \tag{3}$$

where a_0 and c_0 are the equilibrium values of the lattice parameters, $\epsilon_z=(c-c_0)/c_0$ is the strain along the c-axis, and the in-plane strain $\epsilon_x=\epsilon_y=(a-a_0)/a_0$ is assumed to be isotropic. The third independent component of the piezoelectric tensor, e_{15}, is related to the polarization induced by shear strain, and will not be discussed. The relation between the lattice constants of the hexagonal GaN is given to

$$\frac{c-c_0}{c_0}=-2\frac{C_{13}}{C_{33}}\frac{a-a_0}{a_0}, \tag{4}$$

where C_{13} and C_{33} are elastic constants (Table II). Using Eqs. (3) and (4), the amount of the piezoelectric polarization in the direction of the c-axis can be determined by

$$P_{\mathrm{PE}}=2\frac{a-a_0}{a_0}\left(e_{31}-e_{33}\frac{C_{13}}{C_{33}}\right). \tag{5}$$

Since $[e_{31}-e_{33}(C_{13}/C_{33})]<0$ for AlGaN over the whole range of compositions, the piezoelectric polarization is negative for tensile and positive for compressive strained barriers, respectively. The spontaneous polarization for GaN and AlN

Downloaded 28 Mar 2002 to 128.111.29.147. Redistribution subject to AIP license or copyright, see http://ojps.aip.org/japo/japcr.jsp

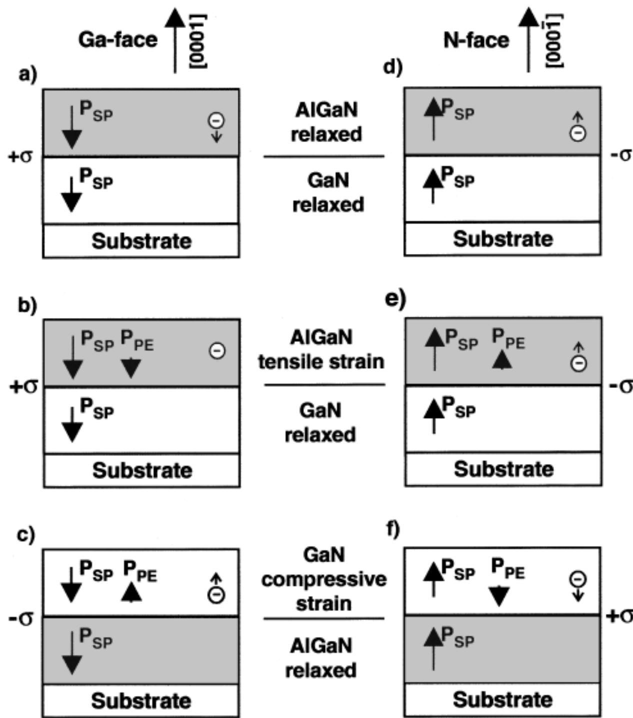

FIG. 7. Polarization induced sheet charge density and directions of the spontaneous and piezoelectric polarization in Ga- and N-face strained and relaxed AlGaN/GaN heterostructures.

was found to be negative,[14] meaning that for Ga(Al)-face heterostructures the spontaneous polarization is pointing towards the substrate (Fig. 7). As a consequence, the alignment of the piezoelectrical and spontaneous polarization is parallel in the case of tensile strain, and antiparallel in the case of compressively strained top layers. If the polarity flips over from Ga-face to N-face material, the piezoelectric, as well as the spontaneous polarization changes its sign. In Fig. 7, the directions of the spontaneous and piezoelectric polarization are given for Ga-face, N-face, strained, unstrained AlGaN/GaN, and GaN/AlGaN heterostructures.

Associated with a gradient of polarization in space is a polarization induced charge density given by $\rho_P = \nabla P$. In analogy, at an abrupt interface of a top/bottom layer (AlGaN/GaN or GaN/AlGaN) heterostructure the polarization can decrease or increase within a bilayer, causing a polarization sheet charge density defined by

$$\sigma = P(\text{top}) - P(\text{bottom}) = \{P_{\text{SP}}(\text{top}) + P_{\text{PE}}(\text{top})\} - \{P_{\text{SP}}(\text{bottom}) + P_{\text{PE}}(\text{bottom})\}. \quad (6)$$

Although, variations in composition, surface roughness, or strain distribution will alter the local distribution of polarization induced sheet charge density. However, the total sheet charge, which is associated with the change of polarization across the interface region will be very nearly equal to that present at an abrupt interface. If the polarization induced sheet charge density is positive $(+\sigma)$, free electrons will tend to compensate the polarization induced charge, e.g., during the cooling process after growth. These electrons will form a 2DEG with a sheet carrier concentration n_S, assuming that the AlGaN/GaN band offset is reasonably high and that the interface roughness is low. A negative sheet charge density $(-\sigma)$ will cause an accumulation of holes at the interface. For a Ga(Al)-face AlGaN on top of GaN heterostructure (as calculated in detail later on), the polarization induced sheet charge is positive [Fig. 7(a)]. Even if the heterostructure is relaxed (AlGaN thickness $\gg$65 nm), electrons will be confined at the interface because of the difference in spontaneous polarization of GaN and AlGaN. If this heterostructure is grown pseudomorphic [Fig. 7(b)] the piezoelectric polarization of the tensile strained AlGaN barrier will increase the difference $P(\text{AlGaN})$-$P(\text{GaN})$, and likewise the sheet charge $+\sigma$ and the sheet carrier concentration n_S. For N-face AlGaN/GaN heterostructures, the spontaneous and piezoelectric polarization have opposite directions in comparison to the Ga-face structure. The polarization induced sheet charge is negative, and holes can be accumulated at this interface [Figs. 7(d) and 7(e)]. In N-face heterostructures, electrons will be confined if GaN is grown on top of AlGaN, due to the positive sheet charge which will be formed in this case [Fig. 7(f)]. Following this argument, it becomes obvious why a 2DEG is detected by Hall-effect and the *C–V*-profiling technique at the AlGaN/GaN interface of structure A but not in structure B (Fig. 1). Because of the different polarities of the MOCVD (Ga(Al)-face) and PIMBE (N-face) grown samples, a positive sheet charge which is compensated by electrons 2DEG has to be expected for heterostructure A and a negative sheet charge causing hole accumulation at the interface of structure B. The N-face heterostructure C grown by PIMBE contains a GaN/AlGaN and an AlGaN/GaN interface. In agreement with the given arguments, the 2DEG is detected at the upper GaN/AlGaN $(+\sigma)$ and not at the lower AlGaN/GaN $(-\sigma)$ interface.

To calculate the amount of the polarization induced sheet charge density σ at the AlGaN/GaN and GaN/AlGaN interfaces in dependence of the Al-content x of the $Al_xGa_{1-x}N$ barrier, we use the following set of linear interpolations between the physical properties of GaN and AlN: lattice constant:

$$a(x) = (-0.077x + 3.189)10^{-10}\ \text{m}, \quad (7)$$

elastic constants:

$$C_{13}(x) = (5x + 103)\ \text{GPa}, \quad (8)$$

$$C_{33}(x) = (-32x + 405)\ \text{GPa}, \quad (9)$$

piezoelectric constants:

$$e_{31}(x) = (-0.11x - 0.49)\ \text{C/m}^2, \quad (10)$$

$$e_{33}(x) = (0.73x + 0.73)\ \text{C/m}^2, \quad (11)$$

spontaneous polarization:

$$P_{\text{SP}}(x) = (-0.052x - 0.029)\ \text{C/m}^2. \quad (12)$$

The amount of the polarization induced sheet charge density for the undoped pseudomorphic N-face $\text{GaN/Al}_x\text{Ga}_{1-x}\text{N/GaN}$ heterostructure grown by PIMBE is calculated using Eqs. (5), (6), and (12)

Downloaded 28 Mar 2002 to 128.111.29.147. Redistribution subject to AIP license or copyright, see http://ojps.aip.org/japo/japcr.jsp

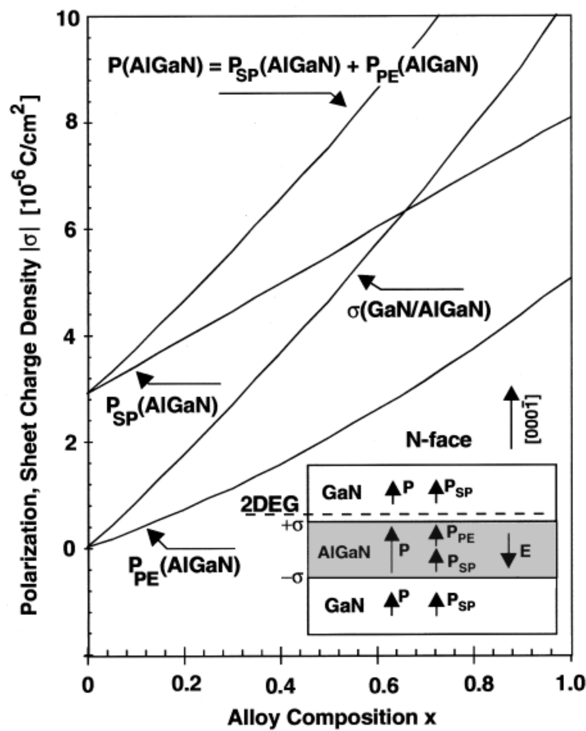

FIG. 8. Spontaneous, piezoelectric, total polarization of AlGaN and sheet charge density at the upper interface of a N-face GaN/AlGaN/GaN heterostructure vs alloy composition of the barrier.

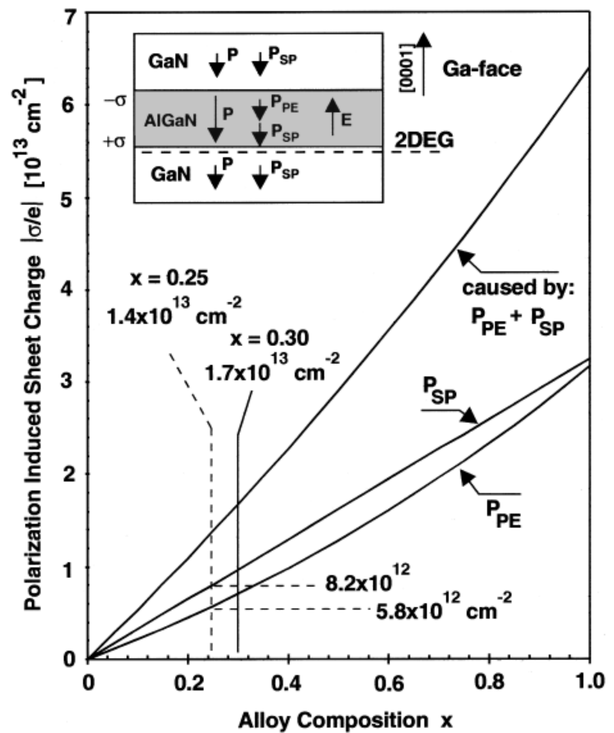

FIG. 9. Calculated sheet charge density caused by spontaneous and piezoelectric polarization at the lower interface of a Ga-face GaN/AlGaN/GaN heterostructure vs alloy composition of the barrier.

$$|\sigma(x)| = |P_{\mathrm{PE}}(\mathrm{Al}_x\mathrm{Ga}_{1-x}\mathrm{N}) + P_{\mathrm{SP}}(\mathrm{Al}_x\mathrm{Ga}_{1-x}\mathrm{N}) - P_{\mathrm{SP}}(\mathrm{GaN})|, \tag{13}$$

$$|\sigma(x)| = \left| 2\,\frac{a(0)-a(x)}{a(x)} \left\{ e_{31}(x) - e_{33}(x)\,\frac{C_{13}(x)}{C_{33}(x)} \right\} + P_{\mathrm{SP}}(x) - P_{\mathrm{SP}}(0) \right|. \tag{14}$$

By increasing the Al-content of the barrier, the piezoelectric and spontaneous polarization of AlGaN are increasing. The sheet charge density caused by the different total polarizations of AlGaN and GaN is increasing slightly more than linear. Increasing the Al-content from $x=0.15$ to 0.3, the calculated sheet charge density increases from $\sigma=0.013$ to $0.027\ \mathrm{C/m^2}$. In Fig. 8, the amount of the spontaneous, piezoelectric, and total polarization of the AlGaN barrier, as well as the sheet charge density at the GaN/AlGaN interface, are shown versus x. For the N-face ([$000\bar{1}$]) heterostructure, the sign of the polarization induced sheet charge is determined to be negative for the lower AlGaN/GaN and positive for the upper GaN/AlGaN interface. Applying Eqs. (5), (6), and (12) to a Ga-face GaN/AlGaN/GaN heterostructure, the amount of the sheet charge density remains the same, but the positive sheet charge causing a 2DEG is located at the lower AlGaN/GaN interface. In Fig. 9, the sheet charge σ/e at the AlGaN/GaN interface caused by the spontaneous and piezoelectric polarization is shown versus alloy composition, proving that the contribution of both kind of polarizations to the sheet charge is nearly the same. For $x=0.18$, a remarkably high sheet charge σ/e of $1\times10^{13}\,\mathrm{cm}^{-2}$, increasing to $1.7\times10^{13}\,\mathrm{cm}^{-2}$ if the Al-content of the barrier is enhanced to $x=0.3$, is determined. These calculated sheet charges located at the AlGaN/GaN interface are about ten times higher than in comparable heterostructures of other III–V heterostructures,[52] thus high polarization induced sheet carrier concentrations may be expected.

V. SHEET CARRIER CONCENTRATION AND MOBILITY

Free electrons tend to compensate the high positive polarization induced sheet charge at the AlGaN/GaN interface for Ga(Al)-face or at the GaN/AlGaN interface for N-face material. The maximum sheet carrier concentration located at these interfaces of the nominally undoped structures is expected to be[11]

$$n_S(x) = \frac{+\sigma(x)}{e} - \left(\frac{\epsilon_0\epsilon(x)}{de^2}\right)[e\phi_b(x) + E_F(x) - \Delta E_C(x)], \tag{15}$$

where d is the width of the $\mathrm{Al}_x\mathrm{Ga}_{1-x}\mathrm{N}$ barrier, $e\Phi_b$ is the Schottky–Barrier of a gate contact, E_F is the Fermi level with respect to the GaN conduction-band-edge energy, and ΔE_C is the conduction band offset at the AlGaN/GaN interface. To determine the sheet carrier concentration from the polarization induced sheet charge density from Eq. (15), we use the following approximations:
dielectric constant:

$$\epsilon(x) = -0.5x + 9.5, \tag{16}$$

Schottky barrier[53]:

$$e\phi_b = (1.3x + 0.84)\ \ \mathrm{eV}, \tag{17}$$

Downloaded 28 Mar 2002 to 128.111.29.147. Redistribution subject to AIP license or copyright, see http://ojps.aip.org/japo/japcr.jsp

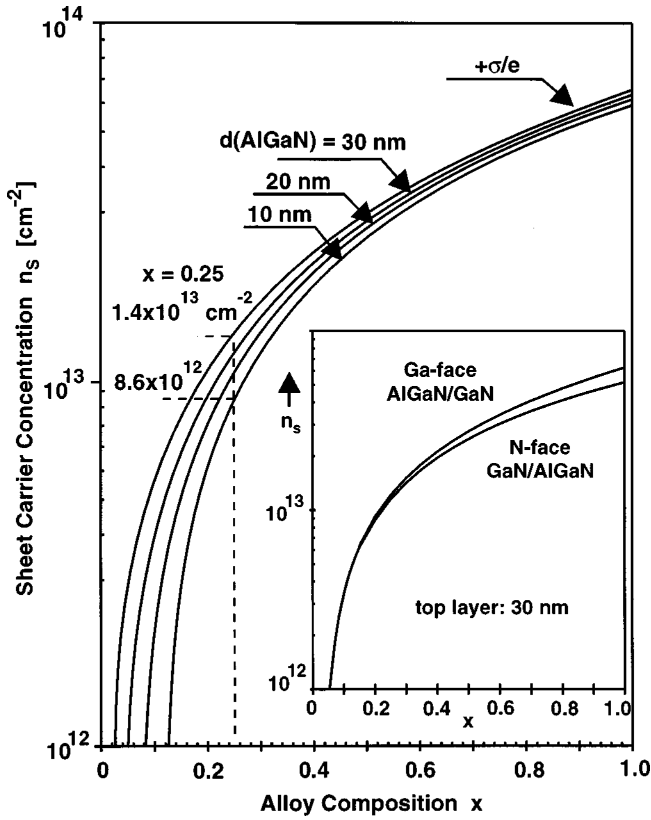

FIG. 10. Sheet carrier concentration of the 2DEG confined at a Ga-face (GaN/)AlGaN/GaN or N-face GaN/AlGaN(/GaN) interface for different thickness of the AlGaN barrier. The insert shows the maximum sheet carrier concentration of a pseudomorphic grown Ga-face AlGaN/GaN and a N-face GaN/AlGaN heterostructure.

Fermi energy[54]:

$$E_F(x)=E_0(x)+\frac{\pi\hbar^2}{m^*(x)}n_S(x),$$

where the ground subband level of the 2DEG is given by

$$E_0(x)=\left\{\frac{9\pi\hbar e^2}{8\epsilon_0\sqrt{8m^*(x)}}\frac{n_S(x)}{\epsilon(x)}\right\}^{2/3}, \tag{18}$$

with the effective electron mass, $m^*(x)\approx 0.22m_e$, band offset[55,56]:

$$\Delta E_C=0.7[E_g(x)-E_g(0)], \tag{19}$$

where the band gap of AlGaN is measured to be[57]

$$E_g(x)=xE_g(\mathrm{AlN})+(1-x)E_g(\mathrm{GaN})-x(1-x)1.0\ \mathrm{eV}, \tag{20}$$

$$=x6.13\ \mathrm{eV}+(1-x)3.42\ \mathrm{eV}-x(1-x)1.0\ \mathrm{eV}. \tag{21}$$

The calculated maximum sheet carrier concentration $n_S(x)$ of the 2DEG located at an AlGaN/GaN interface is shown in Fig. 10. For a constant barrier width of 30 nm, n_S is determined to be 0.92, 1.51, and $2.1\times10^{13}\,\mathrm{cm}^{-2}$ for alloy compositions of $x=0.2$, 0.3, and 0.4, respectively. If the width of an $Al_{0.25}Ga_{0.75}N$ barrier is decreased from 30 over 20 to 10 nm the sheet carrier concentration is lowered from 1.21 over 1.12 to $0.86\times10^{13}\,\mathrm{cm}^{-2}$ in good agreement with the experimental results obtained by $C-V$-profiling. It should be mentioned that the maximum sheet carrier concentration n_S at the interface of a Ga(Al)-face pseudomorphically grown $Al_xGa_{1-x}N$/GaN is equal to the sheet carrier concentration at the GaN/$A_xGa_{1-x}N$ interface (for the same alloy composition of the barrier) of a pseudomorphic grown N-face GaN/AlGaN/GaN heterostructure (realized in this work), but n_S located at the interface of N-face pseudomorphic grown GaN on top of relaxed $Al_xGa_{1-x}N$ will be slightly lower due to the smaller piezoelectric constants of GaN in comparison to AlGaN (see insert of Fig. 10 and Table IV).

To prove our interpolation model for the calculation of the piezoelectric and spontaneous polarization used to explain the very high sheet carrier concentration, we compare the calculated maximum sheet carrier density versus Al-content ($d(\mathrm{AlGaN})=30\,\mathrm{nm}$) with the sheet carrier concentration experimentally determined by Hall-effect and $C-V$-measurements presented above. These data are shown in Fig. 11 for undoped and doped AlGaN/GaN based heterostructures suitable for the fabrication of high quality and high power HFETs.[6,17,58–63] Between barrier alloy compositions of $x=0.15$ and 0.3, we find an excellent agreement of the calculated and measured sheet carrier concentrations of undoped AlGaN/GaN heterostructures (Fig. 11, black symbols). Even for Si-doped barriers (open symbols), the measured sheet carrier concentrations are very close to the maximum sheet carrier concentrations compensating the polarization induced sheet charge. Heterostructures containing AlGaN barriers with $x>0.4$ and $x<0.15$ are not applicable for high quality HFETs to date. For $x>0.4$, the high lattice

TABLE IV. Calculated stress, polarization, electric field, sheet charge density, and sheet carrier density of relaxed and strained Ga-face and N-face AlGaN/GaN heterostructures.

Top/bottom layer	Face	Stress	Strain 10^{-3}	P_{SP} $10^{-6}\,C/\mathrm{cm}^2$	P_{PE} $10^{-6}\,C/\mathrm{cm}^2$	σ $10^{-6}\,C/\mathrm{cm}^2$	E $10^6\,V/\mathrm{cm}$	n_s $10^{13}\,\mathrm{cm}^{-2}$
AlGaN/GaN $x=0.3$	Ga	Relaxed	0	−4.5	0	1.6	1.36	*e* 0.83
	N	Relaxed	0	4.5	0	−1.6	−1.36	*h*
AlGaN/GaN $x=0.3$	Ga	Tensil	7.3	−4.5	−1.1	2.7	6.8	*e* 1.51
	N	Tensil	7.3	4.5	1.1	−2.7	−6.8	*h*
GaN/AlGaN $x=0.3$	Ga	Compress.	−7.2	−2.9	0.97	−2.5	−2.29	*h*
	N	Compress.	−7.2	2.9	−0.97	2.5	2.29	*e* 1.42

Downloaded 28 Mar 2002 to 128.111.29.147. Redistribution subject to AIP license or copyright, see http://ojps.aip.org/japo/japcr.jsp

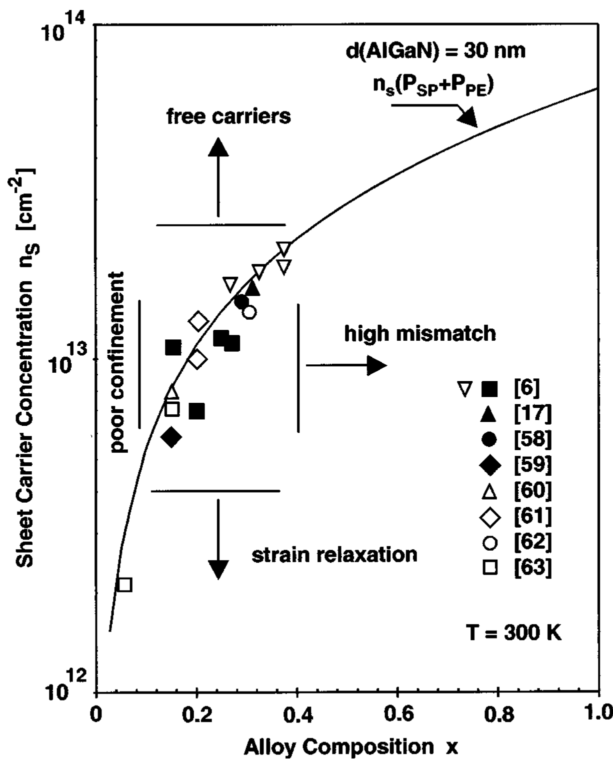

FIG. 11. Calculated and measured sheet carrier concentrations vs Al-content of the AlGaN barrier layer.

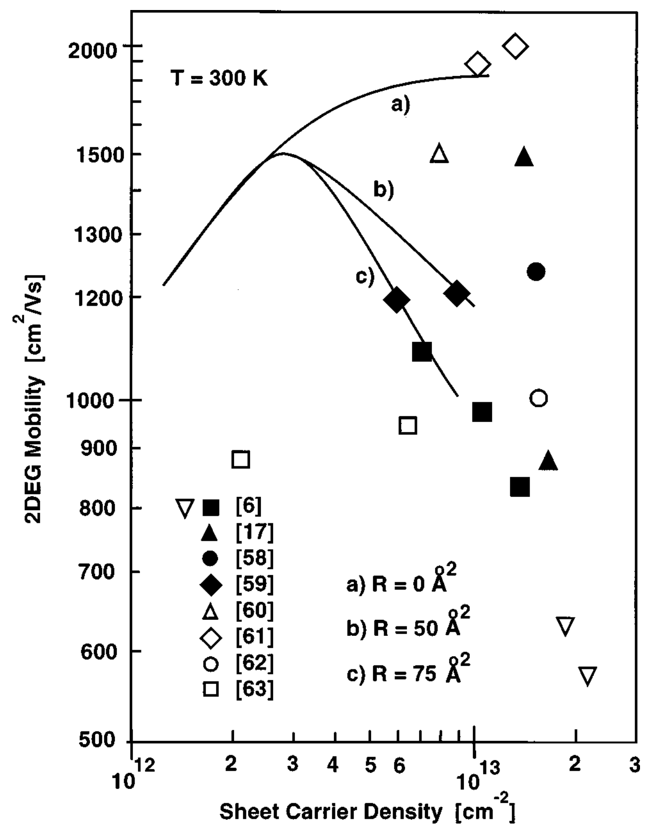

FIG. 12. Calculated (see Ref. 65) and measured 2DEG mobility vs sheet carrier concentrations for different AlGaN/GaN interface roughnesses.

and thermal mismatch between the GaN buffer and the barrier layer are causing a high density of structural defects in the AlGaN, and rough interfaces limiting the 2DEG mobility. For $x<0.15$, the conduction band offset becomes small ($\Delta E_C<0.28$ eV), resulting in bad confinement of the polarization induced sheet carrier concentration. Significant deviations of the measured sheet carrier concentrations by Hall-effect or $C-V$-profiling from the calculated values can be caused by free carrier concentrations in the GaN buffer layer, unintentional doping of the barrier (n_S will be higher),[64] or strain relaxation of the barrier (n_S will be lower).

Knowing the maximum sheet carrier concentration $n_S(x)$ at the interface of undoped AlGaN/GaN structures, one can estimate the minimum sheet resistivity $\rho_{2\mathrm{DEG}}(x)$ to

$$\rho_{2\mathrm{DEG}}(x)=\frac{1}{en_S(x)\mu_s(x)}, \tag{22}$$

where $\mu_s(x)$ is the drift mobility of electrons in the 2DEG. The drift mobility calculated by Oberhuber *et al.*[65] is shown in Fig. 12 together with experimental results as a function of sheet carrier concentration and as a function of interface roughness R. The latter may be characterized by a product of step height and correlation length.[66]

At room temperature, the maximum electron mobility is limited by polar optical phonon scattering. At low sheet carrier densities, impurity and piezoacoustic scattering diminish the mobility. For higher densities, these scattering processes are screened, which explains the increase in mobility up to 2000 cm^2/V s for $n_S>10^{13}\,\mathrm{cm}^{-2}$. At very high sheet carrier densities, the average distance of the 2DEG to the AlGaN/GaN interface becomes smaller (only 2 nm for $n_s=10^{13}\,\mathrm{cm}^{-2}$). Depending on the interface quality, this can decrease the mobility significantly due to the increase in interface roughness scattering shown in Fig. 12.[65]

The minimum sheet resistivity versus alloy composition is shown in Fig. 13 for different interface roughnesses. For an ideal interface in an AlGaN/GaN based HFET, the calculated sheet resistivity lies between 300 and 190 Ω for Al contents between 0.2 and 0.3. The lowest reported sheet resistivities for Al contents of the barrier layer between 0.2 and 0.3 are between 400 and 200 Ω.[59–63] The experimentally observed slightly higher sheet resistivities can be caused by interface roughness scattering or by scattering due to dislocations,[67] which were not taken into account in this work.

The calculated and experimental results show that 2DEGs are generated by spontaneous and piezoelectric polarization effects with sheet resistivities suitable for high frequency and high power HFETs without doping of the barrier layer.

VI. SUMMARY

We have investigated the formation of 2DEGs at interfaces of pseudomorphic wurtzite AlGaN/GaN/AlGaN and GaN/AlGaN/GaN heterostructures grown by MOCVD and PIMBE. For heterostructures with Ga(Al)-face polarity deposited by MOCVD, the 2DEG is located at the interface where AlGaN is grown on top of GaN, whereas in MBE grown samples, determined to be N-face, the electrons are confined at the interface where GaN is grown on top of Al-

Downloaded 28 Mar 2002 to 128.111.29.147. Redistribution subject to AIP license or copyright, see http://ojps.aip.org/japo/japcr.jsp

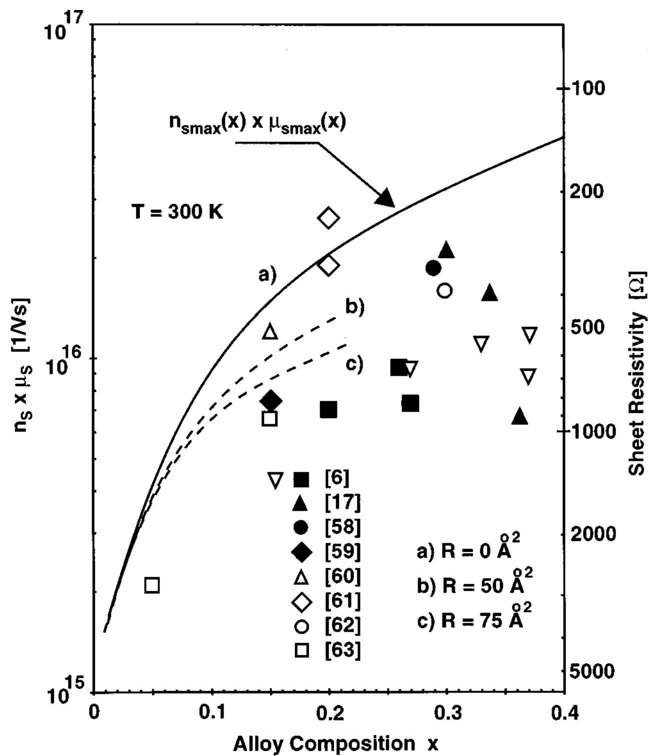

FIG. 13. Calculated and measured 2DEG mobility sheet carrier concentrations products and sheet resistivities for different AlGaN/GaN interface roughnesses.

GaN. By Hall-effect and C–V-profiling techniques the sheet carrier concentration of the 2DEG located at the AlGaN/GaN (Ga-face) and GaN/AlGaN interfaces is measured to increase from 6×10^{12} to $2\times10^{13}\,\mathrm{cm}^{-2}$, if the Al-content of the barrier is increased from $x=0.15$ to 0.31. For a given polarity, the confinement of electrons at specific interfaces and the measured high sheet carrier concentrations can be explained by a compensation of a positive polarization induced sheet charge with a high free carrier density. This sheet charge is caused by different spontaneous and piezoelectric polarizations of the GaN channel and the AlGaN barrier. Because of the increasing spontaneous and piezoelectric polarization of AlGaN with increasing Al-content, the calculated sheet carrier concentration of the 2DEG is increased to $1.67\times10^{13}\,\mathrm{cm}^{-2}$ for $x=0.3$ in good agreement with the experimental results.

The minimum sheet resistivity for intentionally undoped AlGaN/GaN heterostructures containing barriers with alloy composition between $x=0.2$ and 0.3 is determined to be 300 and 190 Ω. The high thermal stability, high saturation velocity, high sheet carrier concentration, and low sheet resistivity of Ga-face AlGaN/GaN and N-face GaN/AlGaN heterostructures, make these undoped structures very suitable for high power and high frequency hetero field effect transistors.

ACKNOWLEDGMENTS

Some of the experiments discussed in this article were performed in collaboration with A. Kazimirov, G. Scherb, J. Zegenhagen, T.-L. Lee, M. J. Bedzyk, and M. K. Kelly. The authors would like to thank the Alexander von Humboldt Stiftung for a Feodor Lynen fellowship, and to acknowledge financial support from the Deutsche Forschungsgemeinschaft (Stu 139/2). The work done at Cornell University is supported by the Office of Naval Research under Contract Nos. N00014-96-1-1223 and N00014-95-1-0926 under the direction of Dr. J. Zolper.

[1] A. Ozgur, W. Kim, Z. Fan, A. Botchkarev, A. Salvador, S. N. Mohammad, B. Sverdlov, and H. Morkoc, Electron. Lett. **31**, 1389 (1995).
[2] M. A. Khan, Q. Chen, M. S. Shur, B. T. MsDermott, J. A. Higgins, J. Burm, W. J. Schaff, and L. F. Eastman, IEEE Electron Device Lett. **17**, 584 (1996).
[3] S. C. Binari, J. M. Redwing, G. Kelner, and W. Kruppa, Electron. Lett. **33**, 242 (1997).
[4] R. Gaska, Q. Chen, J. Yang, A. Osinsky, M. A. Khan, and M. S. Shur, IEEE Electron Device Lett. **18**, 492 (1997).
[5] Y. F. Wu, S. Keller, P. Kozodoy, B. P. Keller, P. Parikh, D. Kapolnek, S. P. DenBaars, U. K. Mishra, IEEE Electron Device Lett. **18**, 290 (1997).
[6] R. Dimitrov, L. Wittmer, H. P. Felsl, A. Mitchell, O. Ambacher, and M. Stutzmann, Phys. Status Solidi A **168**, 7 (1998).
[7] E. A. Caridi, T. Y. Chang, K. W. Goosen, and L. F. Eastman, Appl. Phys. Lett. **56**, 659 (1990).
[8] W. Q. Chen and S. K. Hark, J. Appl. Phys. **77**, 5747 (1995).
[9] A. Bykhovski, B. L. Gelmont, and M. S. Shur, J. Appl. Phys. **81**, 6332 (1997).
[10] P. M. Asbeck, E. T. Yu, S. S. Lau, G. J. Sullivan, J. Van Hove, and J. M. Redwing, Electron. Lett. **33**, 1230 (1997).
[11] E. T. Yu, G. J. Sullivan, P. M. Asbeck, C. D. Wang, D. Qiao, and S. S. Lau, Appl. Phys. Lett. **71**, 2794 (1997).
[12] M. B. Nardelli, K. Rapcewicz, and J. Bernholc, Appl. Phys. Lett. **71**, 3135 (1997).
[13] T. Takeuchi, H. Takeuchi, S. Sota, H. Sakai, H. Amano, and I. Akasaki, Jpn. J. Appl. Phys., Part 2 **36**, L177 (1997).
[14] F. Bernardini, V. Fiorentini, and D. Vanderbilt, Phys. Rev. B **56**, 10024 (1997).
[15] W. Zhong, R. D. King-Smith, and D. Vanderbilt, Phys. Rev. Lett. **72**, 3618 (1994).
[16] A. Hangleiter, J. S. Im, H. Kollmer, S. Heppel, J. Off, and F. Scholz, MRS Internet J. Nitride Semicond. Res. **3**, 15 (1998).
[17] J. A. Smart, A. T. Schremer, N. G. Weimann, O. Ambacher, L. F. Eastman, and J. R. Shealy, Appl. Phys. Lett. (submitted).
[18] *Properties of Group III Nitrides*, edited by J. H. Edgar (INSPEC, London, 1994).
[19] K. Tsubouchi, K. Sugai, and N. Mikoshiba, IEEE Ultrason. Symp. **1**, 375 (1981).
[20] A. F. Wright, J. Appl. Phys. **82**, 2833 (1997).
[21] Y. Takagi, M. Ahart, T. Azuhato, T. Sota, K. Suzuki, and S. Nakamura, Physica B **219&220**, 547 (1996).
[22] A. V. Sheleg and V. A. Savastenko, Neorg. Mater. **15**, 1598 (1979).
[23] K. Kim, W. R. L. Lambrecht, and B. Segall, Phys. Rev. B **53**, 16310 (1996).
[24] T. Takeuchi, H. Takeuchi, S. Sota, H. Sakai, H. Amano, and I. Akasaki, Jpn. J. Appl. Phys., Part 2 **36**, L177 (1997).
[25] H. Angerer *et al.*, Appl. Phys. Lett. **71**, 1504 (1997).
[26] J. W. Matthews and A. E. Blakeslee, J. Cryst. Growth **32**, 265 (1974).
[27] A. Fischer, H. Kuhne, and H. Richter, Phys. Rev. Lett. **73**, 2712 (1994).
[28] H. Amano, T. Takeuchi, S. Sota, H. Sakai, and I. Akasaki, Mater. Res. Soc. Symp. Proc. **449**, 1143 (1997).
[29] E. S. Hellman, MRS Internet J. Nitride Semicond. Res. **3**, 11 (1998).
[30] B. Daudin, J. L. Rouviére, and M. Arley, Appl. Phys. Lett. **69**, 2480 (1996).
[31] M. Seelmann-Eggebert, J. L. Weyher, H. Obloh, H. Zimmermann, A. Rar, and S. Porowski, Appl. Phys. Lett. **71**, 2635 (1997).
[32] A. R. Smith, R. M. Feenstra, D. W. Greve, J. Neugebauer, and J. E. Northrup, Phys. Rev. Lett. **79**, 3934 (1997).
[33] A. R. Smith, R. M. Feenstra, D. W. Greve, M. S. Shin, M. Skowronski, J. Neugebauer, and J. E. Northrup, Appl. Phys. Lett. **72**, 2114 (1998).
[34] J. L. Weyher, S. Müller, I. Grzegory, and S. Porowski, J. Cryst. Growth **182**, 17 (1997).
[35] T. Sasaki and T. Matsuoka, J. Appl. Phys. **64**, 4531 (1998).
[36] B. W. Batterman, Phys. Rev. Lett. **22**, 703 (1969).
[37] P. Trucano, Phys. Rev. B **13**, 2524 (1976).

Downloaded 28 Mar 2002 to 128.111.29.147. Redistribution subject to AIP license or copyright, see http://ojps.aip.org/japo/japcr.jsp

[38] T. Takahashi and S. Kikuta, J. Phys. Soc. Jpn. **47**, 620 (1979).
[39] S. Annaka, T. Takahashi, and S. Kikuta, Jpn. J. Appl. Phys., Part 1 **23**, 1637 (1984).
[40] J. R. Patel and J. A. Golovchenko, Phys. Rev. Lett. **50**, 1858 (1983).
[41] A. Kazimirov, G. Scherb, J. Zegenhagen, T.-L. Lee, M. J. Bedzyk, M. K. Kelly, H. Angerer, and O. Ambacher, J. Appl. Phys. **84**, 1703 (1998).
[42] R. Dingle, H. L. Stormer, A. C. Gossard, and W. Wiegmann, Appl. Phys. Lett. **33**, 665 (1978).
[43] J. P. Bergman, Q. X. Zhao, P. O. Holtz, B. Monemar, M. Sundaram, J. L. Merz, and A. C. Gossard, Phys. Rev. B **43**, 4771 (1991).
[44] C. O. Thomas, D. Kahng, and R. C. Manz, J. Electrochem. Soc. **109**, 1055 (1962).
[45] E. F. Schubert, *Doping in III-V Semiconductors* (Cambridge University Press, Cambridge 1993), p. 492.
[46] H. Kroemer, W.-Y. Chien, J. S. Harris Jr., and D. D. Edwall, Appl. Phys. Lett. **36**, 295 (1980).
[47] K. Tsubouchi, N. Miskoshiba, IEEE Trans. Sonics Ultrason. **SU-32**, 634 (1985).
[48] G. D. O'Clock and M. T. Duffy, Appl. Phys. Lett. **23**, 55 (1973).
[49] M. A. Littlejohn, J. R. Hauser, and T. H. Glisson, Appl. Phys. Lett. **26**, 625 (1975).
[50] A. D. Bykhovski, B. L. Gelmont, and M. S. Shur, J. Appl. Phys. **81**, 6332 (1997).
[51] A. S. Barker Jr. and M. Ilegems, Phys. Rev. B **7**, 743 (1973).
[52] W. Q. Chen and S. K. Hark, J. Appl. Phys. **77**, 5747 (1995).
[53] L. S. Yu, D. J. Qiao, Q. J. Xing, S. S. Lau, K. S. Boutros, and J. M. Redwing, Appl. Phys. Lett. **73**, 238 (1998).
[54] M. S. Shur, Mater. Res. Soc. Symp. Proc. **483**, 15 (1998).
[55] G. Martin, S. Strite, A. Botchkaev, A. Agarwal, A. Rockett, H. Morkoc, W. R. L. Lambrecht, and B. Segall, Appl. Phys. Lett. **65**, 610 (1994).
[56] G. Martin, A. Botchkarev, A. Rockett, and H. Morkoc, Appl. Phys. Lett. **68**, 2541 (1996).
[57] D. Brunner, H. Angerer, E. Bustarret, R. Höpler, R. Dimitrov, O. Ambacher, and M. Stutzmann, J. Appl. Phys. **82**, 5090 (1997).
[58] W. J. Schaff *et al.*, presented at 5th Nitride Workshop St. Louis, Missouri, 4–7 August 1998.
[59] S. C. Binari, J. M. Redwing, G. Kelner and W. Kruppa, Electron. Lett. **33**, 242 (1997).
[60] Y.-F. Wu, B. P. Keller, S. Keller, D. Kapolnek, P. Kozodoy, S. P. DenBaars, and U. K. Mishra, Appl. Phys. Lett. **69**, 1438 (1996).
[61] R. Gaska, A. Osinsky, J. W. Yang, and M. S. Shur, IEEE Electron Device Lett. **19**, 89 (1998); R. Gaska, J. W. Yang, A. Osinsky, Q. Chen, M. A. Khan, A. O. Orlov, G. L. Snider, and M. S. Shur, Appl. Phys. Lett. **72**, 707 (1998).
[62] C. Nguyen, N. X. Nguyen, M. Le, and D. E. Grider, Electron. Lett. **34**, 309 (1998).
[63] L. W. Wong, S. J. Cai, R. Li, K. Wang, H. W. Jiang, and M. Chen, Appl. Phys. Lett. **73**, 1391 (1998).
[64] M. A. Khan, J. M. Van Hove, J. N. Kuzina, and D. T. Olson, Appl. Phys. Lett. **58**, 2408 (1991).
[65] R. Oberhuber, G. Zandler, and P. Vogl, Appl. Phys. Lett. **73**, 818 (1998).
[66] R. M. Fenstra and M. A. Lutz, J. Appl. Phys. **78**, 6091 (1995).
[67] N. G. Weimann, L. F. Eastman, D. Doppalapudi, H. M. Ng, and T. D. Moustakas, J. Appl. Phys. **83**, 3656 (1998).

Downloaded 28 Mar 2002 to 128.111.29.147. Redistribution subject to AIP license or copyright, see http://ojps.aip.org/japo/japcr.jsp